

Finite Element Analysis of Thermoelastodynamic Instability Involving Frictional Heating

Yun-Bo Yi

Department of Engineering,
University of Denver,
Denver, CO 80208

A finite element method is used to solve the problem involving thermoelastodynamic instability (TEDI) in frictional sliding systems. The resulting matrix equation contains a complex eigenvalue that represents the exponential growth rate of temperature, displacement, and velocity fields. Compared to the thermoelastic instability (TEI) in which eigenmodes always decay with time when the sliding speed is below a critical value, numerical results from TEDI have shown that some of the modes always grow in the time domain at any sliding speed. As a result, when the inertial effect is considered, the phenomenon of hot spotting can actually occur at a sliding speed below the critical TEI threshold. The finite element method presented here has obvious advantages over analytical approaches and transient simulations of the problem in that the stabilities of the system can be determined for an arbitrary geometry without extensive computations associated with analytical expressions of the contact condition or numerical iterations in the time domain. [DOI: 10.1115/1.2345412]

Keywords: thermoelastic, thermoelastodynamic, instability, finite element

1 Introduction

Instabilities in frictional sliding systems can cause vibration and hot spotting and impose design constraints on many high performance systems [1]. The investigation of the problem, both experimentally and numerically, has a long history. However, the explanations on the mechanism vary.

For low frequency vibrations in the unstable system, it is believed that the feedback process between thermoelastic deformation and frictional heating is the primary source. The earliest work in this field can be traced back to Barber [2,3], who conducted a detail investigation on the mechanism for thermoelastic instability (TEI). This work laid ground for later investigation on the phenomenon in both experiments and numerical simulations. Anderson and Knapp [4], for example, characterized in experiments different types of hot spotting as a result of thermoelastic instability in automotive brake systems. The numerical treatment of the TEI problem typically involved Burton's perturbation method [5], in which the temperature field is expressed in a perturbed form with an exponentially growing rate. This method has been used extensively in both analytical approaches (Lee and Barber [6]) and finite element methods (Yi et al. [7]) for exploring the problem's characteristic properties. In addition to the perturbation method, direct transient simulations on the thermoelastic effects were also performed in various research groups (Zagrodzki et al. [8]; Kennedy and Ling [9], Afferrante et al. [10]). However, due to the intensive computations for iterations in the time domain, the transient modeling is only applicable to relatively simple geometries such as one dimensional rod or two-dimensional layers.

On the other hand, dynamic instabilities associated with "squeals" phenomena are well known to occur in frictional contact leading to stick-slip or other high frequency oscillations. For example, Martins et al. [11] and Adams [12] showed that the steady state sliding of two elastic or viscoelastic half planes can be dynamically unstable if the coefficient of friction or Poisson's ratio is sufficiently large. Kincaid et al. [13] found that the transverse motion of the automotive disc brakes experiences a sharp

change in excitation when the slip velocity is low, and that this change can cause a complicated vibration associated with brake squeal. Moirrot et al. [14] also indicated the existence of the stick-slip and stick-slip-separation wave propagation in a brake system using a semianalytical approach. Ouyang et al. [15] investigated the friction-induced vibration and squeal frequencies using both finite element analysis and experiments.

The two mechanisms (thermoelastic instability and dynamic instability) have significantly different time scales and have never been considered coupled: Inertial terms in TEI models are rarely considered and the thermal effects in structural vibration models are always neglected. It is not until recently that researchers started to realize the importance of coupling between thermal and inertial effects. For example, Afferrante et al. [16] used a simple elastic layer model confined between two rigid surfaces and showed that weak coupling between thermoelastic and elastodynamic can actually lead to instabilities at an arbitrarily small sliding speed. The same research group further attempted to solve the problem considering the effect of the shear wave propagation. They showed that when the frictional shear traction is considered for elastic deformation, different boundary conditions can result in four possible categories of problem cases. This new phenomenon has been referred to as "thermoelastodynamic instability" or TEDI.

The main disadvantage of the existing analytical tools for TEDI lies that almost all the models involved have oversimplified geometries such as rods and half planes. Previous researches on thermoelastic problems [17] indicated that geometry can significantly alter the thermal-mechanical behaviors of the system. Although analytical methods are capable of exploring fundamental features of the problem, successful application of the methods to practical problems that typically involve multiple layers of finite thickness is difficult, since it would require extremely time-consuming effort in the numerical iterations. The transient simulation schemes, on the other hand, are possibly manageable in problems in two dimensions but would pose considerable difficulties in the three-dimensional geometry needed to give a realistic approximation to a practical system. The finite element method in contrast provides a powerful tool that has obvious advantages over the other approaches, in that the stabilities of the system can be determined for an arbitrary geometry without extensive com-

Contributed by the Tribology Division of ASME for publication in the JOURNAL OF TRIBOLOGY. Manuscript received January 17, 2006; final manuscript received April 30, 2006. Review conducted by Kwangjin Lee.

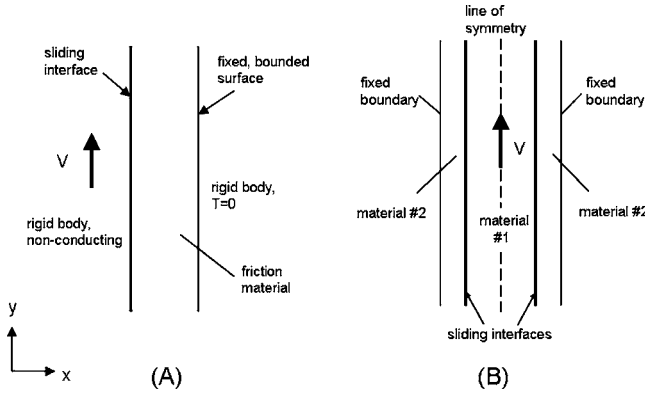


Fig. 1 Schematic of the computational model: (a) An elastic layer sliding against a rigid, nonconducting body (the single-material model); (b) a layer sliding between two elastic and conducting layers (the multi-material model)

putations associated with analytical expressions of the contact condition or numerical iterations in the time domain. Therefore, the proposed finite element scheme is believed among the best solution methods for instability analysis of the problem in interest.

2 Method

To demonstrate the proposed methodology, two simple problems are considered in the present work: (a) A conducting, elastic layer sliding against a rigid, nonconducting body; (b) a conducting, elastic layer (material 1) sliding between two layers of finite thicknesses (material 2), which are also elastic and conducting. The plane-strain condition is assumed in both cases. The schematics of the two models are shown in Fig. 1. The first model is adapted from the one used in Afferrante et al. work [16], for the purpose of comparison and validation. The second model, compared to the first one or any other oversimplified half-plane models employed by researchers in the elasticity community, can better reflect the realistic configuration of a frictional sliding system. In both models, we assume that the contact is conforming, namely, the extent of the contact area does not change with time and there is no separation occurring during the sliding.

2.1 The Heat Transfer Problem. The two-dimensional heat conduction equation for the sliding bodies in the fixed frame of reference x and y can be written as

$$K \left(\frac{\partial^2 T}{\partial x^2} + \frac{\partial^2 T}{\partial y^2} \right) - \rho c \left(\frac{\partial T}{\partial t} + V \frac{\partial T}{\partial y} \right) = 0 \quad (1)$$

where K , ρ , and c are thermal conductivity, density and specific heat, respectively. The sliding takes place in the y direction as shown in Fig. 1. We assume an exponentially growing perturbation solution of the form

$$T(x, y, t) = T_0(x, y) + \Re \{ e^{bt+jmy} \Theta(x) \} \quad (2)$$

where b is a complex exponential growth rate and m is wave number defined as the number of oscillations for perturbation within a length of 2π (m). Note that m can take any positive real value, not necessarily an integer. T_0 is the steady state solution and satisfies the heat conduction equation. \Re represents the real part of a complex number. Substitution of Eq. (2) into Eq. (1) yields

$$K \frac{\partial^2 \Theta}{\partial x^2} - Km^2 \Theta - \rho c (jmV + b) \Theta = 0 \quad (3)$$

Applying the standard Galerkin finite element formulation results in a matrix equation in the following form:

$$(\mathbf{K} + \mathbf{R} + b\mathbf{H})\Theta + \mathbf{Q} = 0 \quad (4)$$

where \mathbf{Q} is the nodal heat flux and the elemental matrices are

$$K_e = \int K \left(\frac{\partial N(x)}{\partial x} \frac{\partial N(x)^T}{\partial x} \right) dx \quad (5)$$

$$R_e = \int (Km^2 + jm\rho cV) N(x) N(x)^T dx \quad (6)$$

$$H_e = \int \rho c N(x) N(x)^T dx \quad (7)$$

where $N(x)$ is the shape function.

2.2 Frictional Heat Generation. The frictional heat generation on the contact interface of the sliding bodies is given by

$$\mathbf{Q} = fVP \quad (8)$$

Where \mathbf{Q} is nodal heat generation rate (heat flux), \mathbf{P} is nodal contact force in the normal direction, and f is the coefficient of Coulumb friction. Please note that in the above equation an approximation has been made for the heat generation: The velocity associated with the frictional heating is assumed to be identical to the sliding speed V . In reality, this speed should be the sliding speed superposed by the local tangential speed on the contact surface. In addition, the friction coefficient f is assumed here independent of temperature.

2.3 Equation of Motion. We have the equation of motion for a two-dimensional elastic body as follows:

$$\frac{\partial \sigma_{xx}}{\partial x} + \frac{\partial \sigma_{xy}}{\partial y} = \rho \frac{\partial^2 u_x}{\partial t^2}; \quad \frac{\partial \sigma_{yy}}{\partial y} + \frac{\partial \sigma_{xy}}{\partial x} = \rho \frac{\partial^2 u_y}{\partial t^2} \quad (9)$$

For simplicity the shear tractions do not appear in the boundary conditions of the contact problem since the effects of shear tractions on normal displacements are negligible. As a result the propagation of shear waves and the dynamic instabilities associated with stick-slip phenomena are not studied in this work.

2.4 Thermoelasticity. For plane-strain problems, the constitutive law for thermoelasticity is

$$\{\sigma_{xx} \quad \sigma_{yy} \quad \sigma_{xy}\}^T = \mathbf{C} \{e_{xx} \quad e_{yy} \quad e_{xy}\}^T - \mathbf{D}T \quad (10)$$

where

$$\mathbf{C} = \frac{E}{(1+\nu)(1-2\nu)} \begin{bmatrix} 1-\nu & \nu & 0 \\ \nu & 1-\nu & 0 \\ 0 & 0 & 1-\nu/2 \end{bmatrix} \quad (11)$$

$$\mathbf{D} = \frac{E\alpha}{(1-2\nu)} \begin{bmatrix} 1 & 1 & 0 \\ 1 & 1 & 0 \\ 1 & 1 & 0 \end{bmatrix} \quad (12)$$

ν is Poisson's ratio; E is elastic modulus, α is coefficient of thermal expansion, and $\{e\}$ is the strain vector, which can be expressed in the matrix form in terms of the nodal displacement vector \mathbf{U} . That is

$$\{e_{xx} \quad e_{yy} \quad e_{xy}\}^T = \mathbf{B}\mathbf{U} \quad (13)$$

By assuming displacement in the perturbation forms as

$$\begin{Bmatrix} u_x(x, y, t) \\ u_y(x, y, t) \end{Bmatrix} = \begin{Bmatrix} u_{x0}(x, y) \\ u_{y0}(x, y) \end{Bmatrix} + \Re \left\{ e^{bt+jmy} \begin{Bmatrix} U_x(x) \\ U_y(x) \end{Bmatrix} \right\} \quad (14)$$

and velocity as

$$\begin{Bmatrix} u'_x(x,y,t) \\ u'_y(x,y,t) \end{Bmatrix} = \begin{Bmatrix} u'_{x0}(x,y) \\ u'_{y0}(x,y) \end{Bmatrix} + \Re \left\{ e^{bt+jmy} \begin{Bmatrix} U'_x(x) \\ U'_y(x) \end{Bmatrix} \right\} \quad (15)$$

and by combining Eqs. (9) and (10), we obtain a matrix equation

$$\mathbf{LU} - \mathbf{G}\Theta = \mathbf{\Phi P} - b\mathbf{SU}' \quad (16)$$

where the elemental matrices

$$\mathbf{L}_e = \int_{\Omega} \mathbf{B}(m,x)^T \mathbf{CB}(m,x) dx, \quad \mathbf{G}_e = \int_{\Omega} \mathbf{B}(m,x)^T \mathbf{DN}(x) dx \quad (17)$$

and

$$\mathbf{B}(m,x) = \begin{bmatrix} dN_1/dx & 0 & dN_2/dx & 0 \\ 0 & mN_1 & 0 & mN_2 \\ -mN_1 & dN_1/dx & -mN_2 & dN_2/dx \end{bmatrix} \quad (18)$$

\mathbf{N}_1 and \mathbf{N}_2 represent the two terms in the shape function \mathbf{N} (note that the finite elements used here are one-dimensional linear elements). Rearrange Eq. (16) in the partitioned form as follows:

$$\begin{bmatrix} \mathbf{L}_1 \\ \mathbf{L}_2 \end{bmatrix} \mathbf{U} - \begin{bmatrix} \mathbf{G}_1 \\ \mathbf{G}_2 \end{bmatrix} \Theta = \begin{bmatrix} \mathbf{I} \\ 0 \end{bmatrix} \mathbf{P} - b \begin{bmatrix} \mathbf{S}_1 \\ \mathbf{S}_2 \end{bmatrix} \mathbf{U}' \quad (19)$$

where \mathbf{I} is the identity matrix of order n_c (the number of contact nodes). Therefore,

$$\begin{aligned} \mathbf{L}_1 \mathbf{U} - \mathbf{G}_1 \Theta + b \mathbf{S}_1 \mathbf{U}' &= \mathbf{P} \\ \mathbf{L}_2 \mathbf{U} - \mathbf{G}_2 \Theta + b \mathbf{S}_2 \mathbf{U}' &= \mathbf{0} \end{aligned} \quad (20)$$

In the above equation, the nodal vectors are partitioned according to whether they are contact nodes or not, this is because each pair of contact nodes has the same normal displacement. In addition, the frictional heat is presumably generated at the contact nodes and consequently the contact nodes have to be treated separately.

2.5 Eigenvalue Equation. Substituting Eqs. (8) and (20) into Eq. (4) yields

$$(\mathbf{K} + \mathbf{C} + f\mathbf{VG}_1)\Theta - f\mathbf{VL}_1\mathbf{U} - bf\mathbf{VS}_1\mathbf{U}' + \mathbf{H} = \mathbf{P} \quad (21)$$

In addition, from Eqs. (14) and (15) we have the relation between the displacement and velocity perturbations as

$$\mathbf{U}' = b\mathbf{U} \quad (22)$$

Combining Eqs. (20)–(22) yields

$$\begin{pmatrix} -(\mathbf{K} + \mathbf{C} + f\mathbf{VG}_1) & f\mathbf{VL}_1 & 0 \\ \mathbf{G}_2 & -\mathbf{L}_2 & 0 \\ 0 & 0 & \mathbf{I} \end{pmatrix} - b \begin{pmatrix} \mathbf{H} & 0 & -f\mathbf{VS}_1 \\ 0 & 0 & \mathbf{S}_2 \\ 0 & \mathbf{I} & 0 \end{pmatrix} \begin{Bmatrix} \Theta \\ \mathbf{U} \\ \mathbf{U}' \end{Bmatrix} = \mathbf{0} \quad (23)$$

or

$$\tilde{\mathbf{A}}\mathbf{X} = b\tilde{\mathbf{B}}\mathbf{X} \quad (24)$$

where

$$\tilde{\mathbf{A}} = \begin{bmatrix} -(\mathbf{K} + \mathbf{C} + f\mathbf{VG}_1) & f\mathbf{VL}_1 & 0 \\ \mathbf{G}_2 & -\mathbf{L}_2 & 0 \\ 0 & 0 & \mathbf{I} \end{bmatrix} \quad (25)$$

$$\tilde{\mathbf{B}} = \begin{bmatrix} \mathbf{H} & 0 & -f\mathbf{VS}_1 \\ 0 & 0 & \mathbf{S}_2 \\ 0 & \mathbf{I} & 0 \end{bmatrix}$$

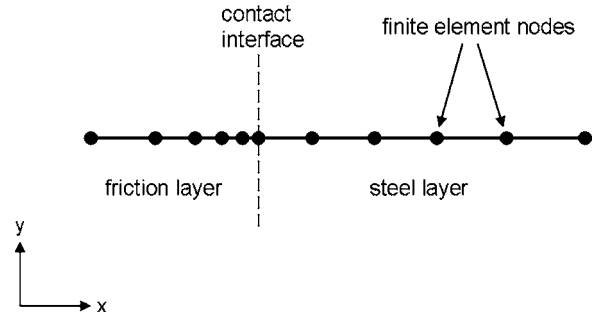


Fig. 2 Biased mesh for modeling the thermal skin layer in the friction material (poor conductor)

$$\mathbf{X} = [\Theta, \mathbf{U}, \mathbf{U}']^T$$

This is a generalized eigenvalue equation. The eigenvalue is the growth rate b and the eigenvector is $[\Theta, \mathbf{U}, \mathbf{U}']^T$, i.e., nodal temperature, displacement, and velocity.

2.6 Meshing Consideration. In the well-characterized thermoelastic instability problem involving two sliding bodies, we know that there is a “thermal skin” in the vicinity of the contact surface of the poor conductor. To improve the accuracy of numerical solution, a graded mesh as shown in Fig. 2 is used in the multi-material model (model B in Fig. 1) to ensure that there are enough elements generated in the thermal skin layer, following the discussion of meshing considerations for materials under high Peclet number by Yi et al. [7]. A bias ratio of the mesh is selected such that

$$\xi \ll 2\pi \sqrt{\frac{2k}{Vm}} \quad (26)$$

where k is thermal diffusivity and ξ is the element length in the normal direction for the element on the sliding surface.

3 Numerical Results

3.1 Single-Material Model. To verify the proposed solution method, analysis was first performed using the single-material model with wave number $m=0$. The steel material properties in Table 1 were used in the analysis. The model geometry and boundary conditions are shown in Fig. 1(a). The real part of the exponential growth rate $\Re(b)$ obtained from the finite element analysis is shown in Fig. 3 as a function of dimensionless sliding speed V^* , which is defined as

Table 1 Material properties used in the finite element analyses

	Steel (material #1)	Friction material (material #2)
Young's modulus, E (Pa)	2.0×10^{11}	3.0×10^8
Poisson's ratio, ν	0.30	0.12
Thermal expansion coefficient, α (K^{-1})	1.2×10^{-5}	1.4×10^{-5}
Thermal conductivity, K ($W m^{-1} K^{-1}$)	42.0	0.241
Thermal diffusivity, k ($m^2 s^{-1}$)	1.2×10^{-5}	1.8×10^{-7}
Density (kg/m^3)	7800	846
Friction coefficient	0.13	0.13
Full thickness (m)	2.75×10^{-3}	6.70×10^{-4}

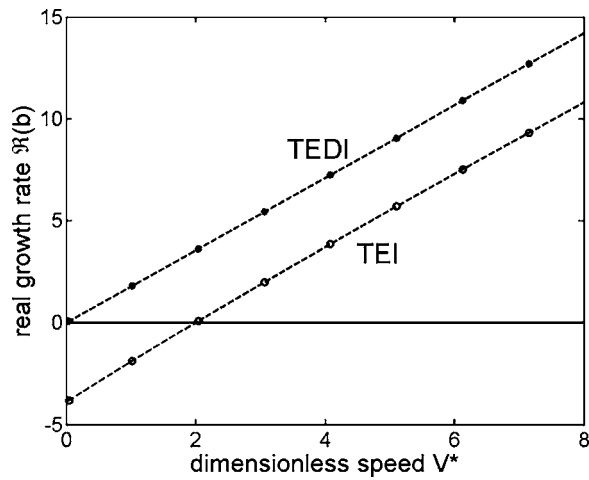


Fig. 3 Real part of the growth rate for dominant eigenmode as a function of dimensionless sliding speed in the single-material model (Fig. 1(a)); $m=0$

$$V^* = \frac{2\mu\alpha(1+\nu)fVh}{K(1-2\nu)} = \frac{E\alpha fVh}{K(1-2\nu)} \quad (27)$$

where μ is shear modulus, h is layer thickness. This definition is consistent with the dimensionless velocity used in Afferrante et al. analytical solutions [16]. The wave number m is set to zero so that the solutions represent the “banding modes” of the system.

In Fig. 3, it is clear that the maximum $\Re(b)$ of the TEDI modes is greater than that of the TEI modes at any sliding speed. In addition, $\Re(b)$ in TEDI is nonzero at an arbitrarily small sliding speed and increases linearly with speed at a rate almost the same as TEI. By contrast, $\Re(b)$ in TEI becomes nonzero only when the sliding speed exceeds a certain threshold, or critical speed. It is also clear that the critical speed for TEI is located exactly at $V^*=2$. These characteristic results are consistent with the analytical solutions reported by Afferrante et al. [16] using the same model geometry and boundary conditions. In addition, the model parameters used in this study (steel material in Table 1) result in the dimensionless parameter $\gamma=7.43 \times 10^{-7} \ll 1$, where

Table 2 Eigenvalues of the leading modes in TEDI

Dominant modes	$V=5 \text{ m/s } (< \text{TEI } V_{cr})$		$V=10 \text{ m/s } (> \text{TEI } V_{cr})$	
	$\Re(b)$	$\Im(b)$	$\Re(b)$	$\Im(b)$
Mode 1	3.68×10^{-5}	$\pm 2.97 \times 10^6$	8.10	-1.96×10^3
Mode 2	8.78×10^{-6}	$\pm 9.04 \times 10^6$	7.68×10^{-6}	$\pm 1.45 \times 10^7$
Mode 3	2.38×10^{-6}	$\pm 2.37 \times 10^9$	4.13×10^{-6}	$\pm 2.90 \times 10^6$

$$\gamma = \frac{k}{h \sqrt{\frac{2\mu(1-\nu)}{\rho(1-2\nu)}}} \quad (28)$$

Therefore, the curves in Fig. 3 correspond to the Afferrante et al. analytical solutions when $\gamma \rightarrow 0$.

3.2 Multi-Material Model. Parametric studies of the problem would involve significant amount of computational work. To illustrate the potential application of the proposed methodology, the three-layer automotive clutch model used by Yi et al. [7] is reconsidered here (see Fig. 2(b)). The problem involves a steel layer sliding between two friction layers. By applying symmetric or antisymmetric boundary conditions, the problem can be reduced to a two-layer model in which a half steel layer is sliding against a friction layer (see Fig. 1). Material and geometries properties are listed in Table 1.

Figure 4 shows the real part of maximum growth rate $\Re(b)$ as a function of sliding velocity V under wave number $m=200 \text{ (m}^{-1}\text{)}$, assuming the model has an antisymmetric boundary condition. $m=200 \text{ (m}^{-1}\text{)}$ has been chosen at the representative wave number under which the system has the lowest critical TEI speed. Compared to Fig. 3, although there exist some similarities (for example, $\Re(b)$ is always positive even at an extremely small sliding speed), we can clearly see the differences between the two figures because different model configurations and material properties are used. The first observation is that the growth rate of TEDI in Fig. 3 is greater than that in Fig. 4 under the same sliding speed. This is because Fig. 4 involves two materials, with the second material much softer than the first one, whereas Fig. 3 involves only one material (the stiffer one). As a result, the overall modulus of the two-material system is reduced and the growth rate increases with speed at a much slower rate. Secondly, TEDI behaves in different fashions in the two figures. In the single material case, the dominant growth rate increases linearly with slid-

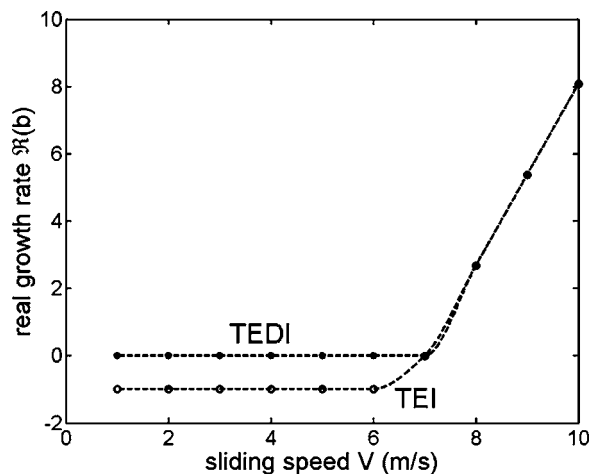


Fig. 4 Real part of the growth rate for dominant eigenmode as a function of sliding speed assuming the antisymmetric boundary condition (multi-material model)

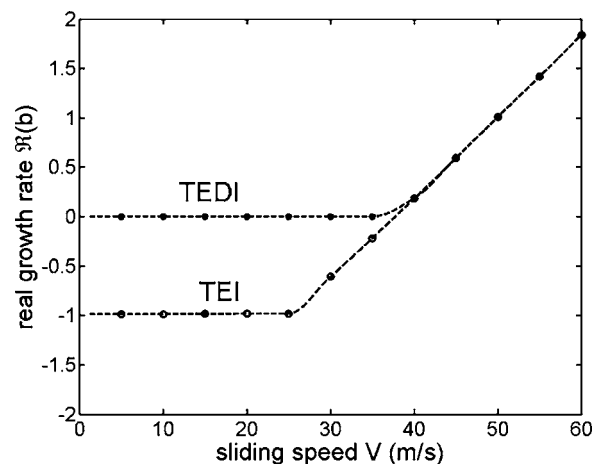


Fig. 5 Real part of the growth rate for dominant eigenmode as a function of sliding speed assuming the symmetric boundary condition (multi-material model)

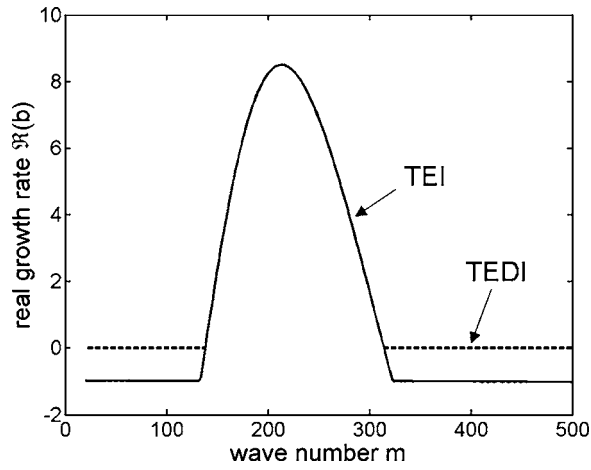


Fig. 6 Comparison of maximum growth rate as a function of wave number m between TEI and TEDI at sliding speed $V = 10$ m/s (above critical TEI speed). Multi-material model under antisymmetric boundary condition is used here.

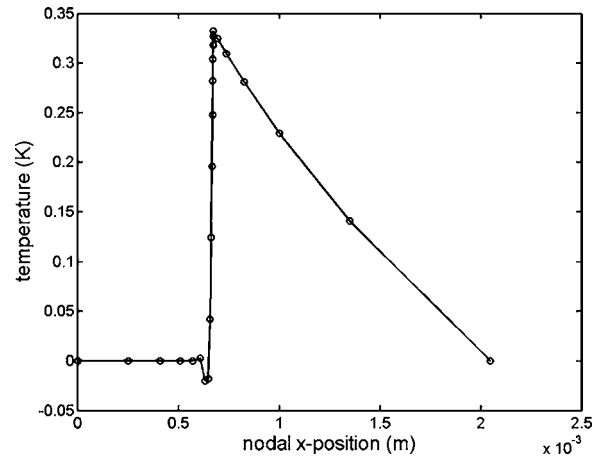


Fig. 7 Profile of temperature eigenvector across the thickness of model for the leading mode under antisymmetric boundary conditions. The wave number m is 200 (m^{-1}).

ing speed whereas in the two-material case, the growth rate keeps almost constant at the beginning and then increases suddenly at some point. This difference is caused by the dissimilarities of the

material properties in the two-material model. When the two materials have similar properties, finite element computations result in smooth curves for growth rate, just as in the single material

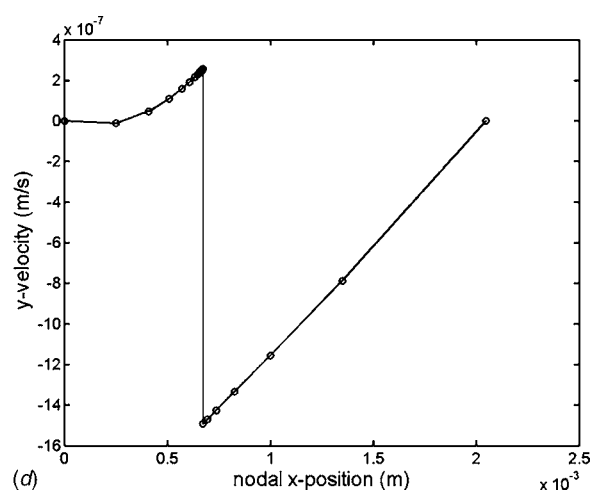
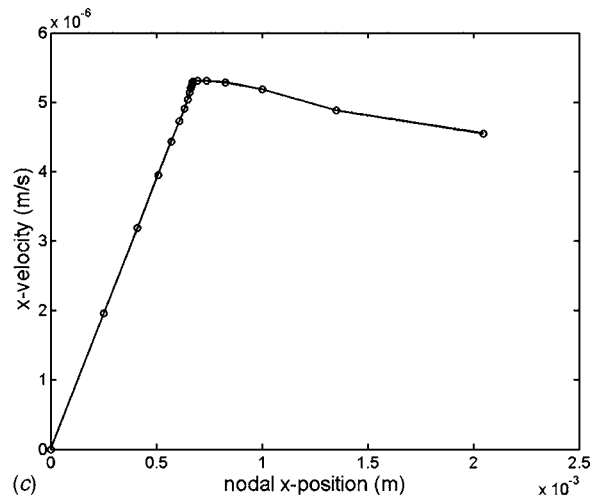
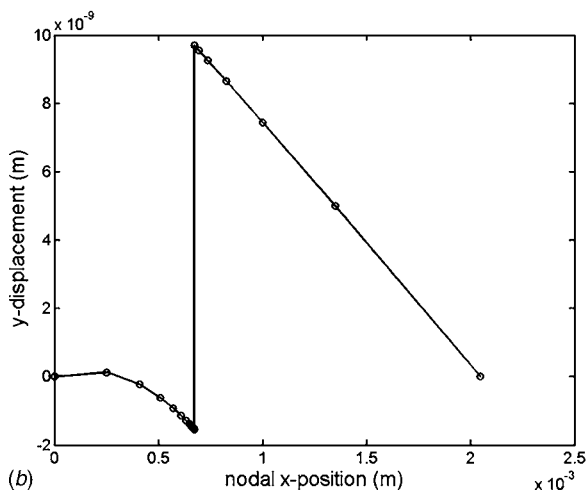
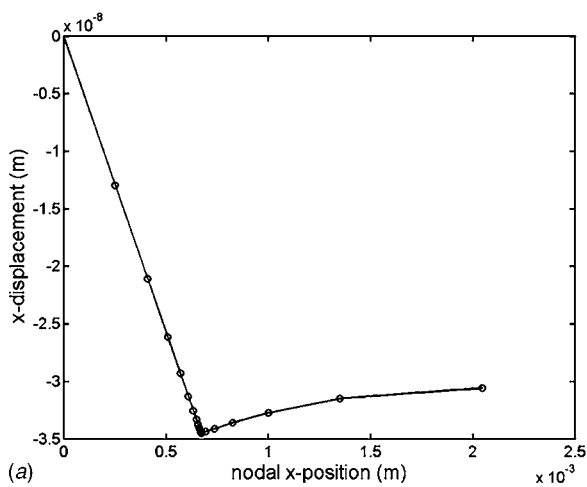


Fig. 8 Profile of displacement/velocity eigenvectors across the thickness of model for the dominant mode assuming the antisymmetric boundary condition. $m=200$ (m^{-1}).

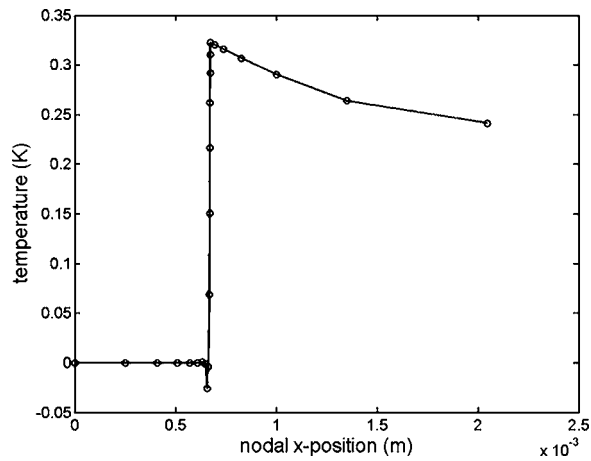


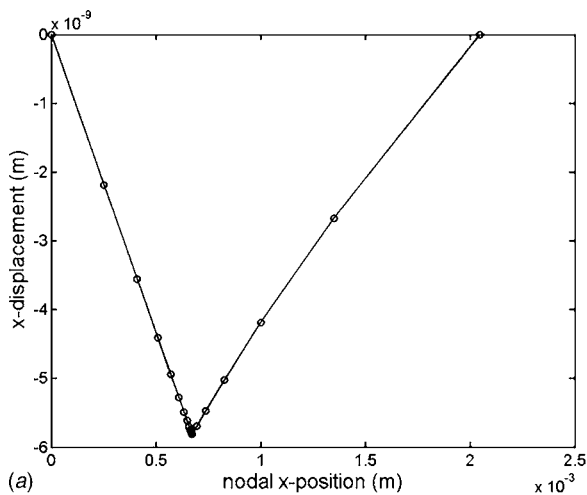
Fig. 9 Profile of temperature eigenvector across the thickness of model for the dominant mode assuming the symmetric boundary condition. $m=200$ (m^{-1}).

case.

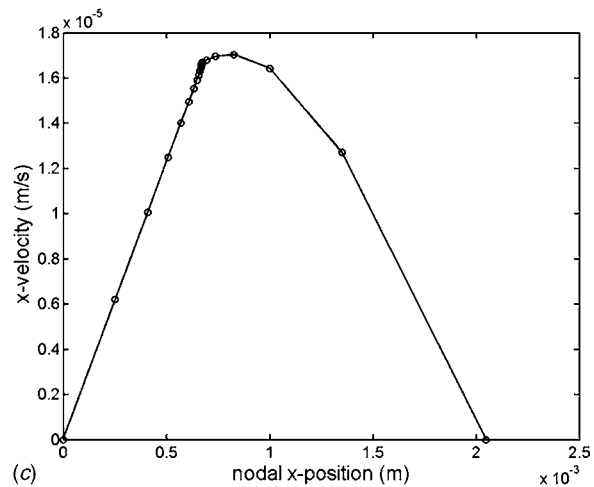
The curve in Fig. 4 can be divided into two distinct phases: In the first phase, the magnitude of $\Re(b)$ is very small (on the order of magnitude approximately 1.0×10^{-5}) and remains independent

of the sliding speed; in the second phase, $\Re(b)$ increases considerably with the sliding speed, following an approximately linear function. The comparison of the same curves between those of TEI and DI reveals that the transition point of the two phases in TEDI corresponds to the “critical sliding speed” in TEI. For pure DI without damping, the eigenmodes correspond to natural vibrations with identically zero growth rates. However, $\Re(b)$ of the leading mode in the first phase of TEDI has the order of magnitude around 1.0×10^{-5} , which is apparently nonzero. Table 2 shows the eigenvalues for some leading modes in TEDI, with both real and imaginary parts tabulated. Investigation on the imaginary part of the growth rate $\Im(b)$ shows that at a sliding speed lower than the TEI critical speed, the leading modes of TEDI vibrate at very high frequencies (Table 2) within the frequency range of the modes induced by DI. (The imaginary growth rates $\Im(b)$ of the DI modes are between 2.54×10^5 and 4.77×10^9 .) This implies that the leading modes at low sliding speeds are induced by dynamic effects, with small but non-negligible growth rates as a result of coupling between DI and TEI. When the sliding speed exceeds the critical TEI speed, the imaginary parts of the leading modes are almost the same as those of TEI modes, showing that the TEI modes now take over and become dominant. The real parts of growth rates for TEI and TEDI are almost identical and do not show appreciably coupling effects in this phase.

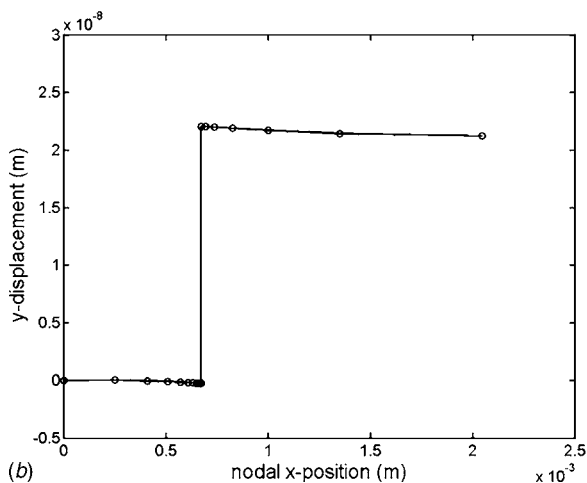
In brief, the results have exhibited some coupling between dynamic instability and thermoelastic feedback at low sliding speed



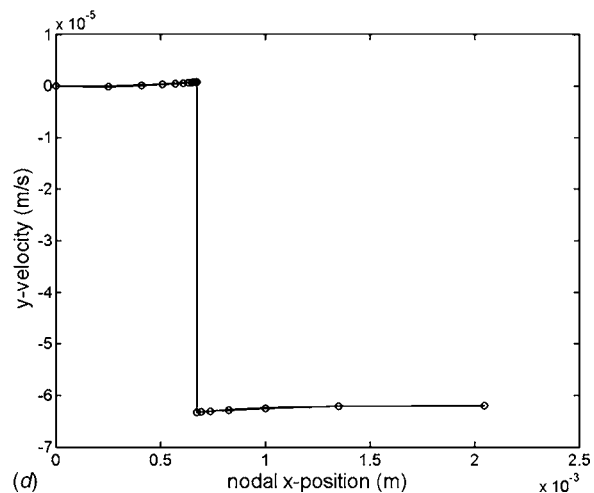
(a)



(c)



(b)



(d)

Fig. 10 Profile of displacement/velocity eigenvectors across the model thickness for the dominant mode assuming the symmetric boundary conditions. $m=200$ (m^{-1}).

but the incorporation of mass does not affect the system instability at high sliding speed where the thermoelastic effects dominate. The inherent reason for that is probably due to the fact that the dynamic modes have natural frequencies much higher than those associated with TEI. It should be pointed out that the curve of $\Re(b)$ for multi-material systems does not always appear like a piece-wise linear curve shown in Fig. 4. When the conductivities of the two materials are sufficiently close, for example, the numerical analysis has shown that the curve becomes nearly parabolic.

Figure 5 shows similar results for the real part of growth rate as a function of sliding velocity, under symmetric boundary condition. Further studies of the results for different wave number m have also shown similar results. For example, Fig. 6 shows a comparison of growth rate as a function of wave number m between TEI and TEDI at sliding speed $V=10$ m/s (above the critical TEI speed), assuming the antisymmetric boundary. Similar results were also obtained from the model assuming symmetric boundary conditions.

Figures 7 and 8 display the eigenvector profiles for temperature, displacement, and velocity under antisymmetric boundaries. The parameters used to compute the eigenvectors are $V=10$ (m/s), $m=200$ (m^{-1}). The temperature profile exhibits strong oscillations in the poor conductor (friction material) whereas there is no oscillation in the good conductor (steel layer), a phenomenon consistent with those observed in TEI. For displacement and velocity profiles, the curve is continuous for U_x and V_x due to the continuity of the normal displacement and velocity on the contact nodes. Whereas the tangential sliding condition on the contact nodes causes discontinuities of U_y and V_y . Eigenvectors under symmetric boundaries are also obtained, as shown in Figs. 9 and 10.

4 Conclusions

A finite element formulation has been established for the problem involving thermoelastodynamic instability. Numerical results show that the dynamic and thermoelastic effects are coupled at low sliding speed in both single-material and multi-material sliding systems but show very weak coupling at speeds above the critical TEI sliding speed in the multi-material systems. The most striking conclusion, however, is that growing modes can always be obtained for TEDI at arbitrarily small sliding speeds and therefore in practical applications, special precautions should be taken on those modes excited at low sliding speed. Compared to analytical resolution and transient simulation of the problem, the finite element method presented here has obvious advantages in that the system stability can be determined for complicated geom-

etries without involving intensive numerical iterations. The same formulation can also be extended to cases in which the boundary conditions are nonuniform, where in most situations analytical solutions would be impractical. Obviously, frictional tractions are not presently included in the current formulation. This would involve too much additional work to include in the present paper. A consequence of this is that one cannot see a pure dynamic instability directly related to "squeal," the instability which happens for a critical friction coefficient, without thermal effects. This challenging topic will be addressed in the future work.

References

- [1] Yi, Y. B., 2001, "Finite Element Analysis of Frictionally Excited Thermoelastic Instabilities in Automotive Brakes and Clutches," Ph.D. Dissertation, University of Michigan, Ann Arbor, Michigan.
- [2] Barber, J. R., 1967, "The Influence of Thermal Expansion on the Friction and Wear Process," *Wear*, **10**, pp. 155–159.
- [3] Barber, J. R., 1969, "Thermoelastic Instabilities in the Sliding of Conforming Solids," *Proc. R. Soc. London, Ser. A*, **312**, pp. 381–394.
- [4] Anderson, A. E., and Knapp, R. A., 1990, "Hot Spotting in Automotive Friction Systems," *Wear*, **135**, pp. 319–337.
- [5] Burton, R. A., Nerlikar, V., and Kilaparti, S. R., 1973, "Thermoelastic Instability in a Seal-Like Configuration," *Wear*, **24**, pp. 177–188.
- [6] Lee, K., and Barber, J. R., 1993, "Frictionally Excited Thermoelastic Instability in Automotive Disk Brakes," *ASME J. Tribol.*, **115**, pp. 607–614.
- [7] Yi, Y. B., Barber, J. R., and Zagrodzki, P., 2000, "Eigenvalue Solution of Thermoelastic Instability Problems Using Fourier Reduction," *Proc. R. Soc. London, Ser. A*, **456**, pp. 2799–2821.
- [8] Zagrodzki, P., Lam, K. B., Al-Bahkali, E., and Barber, J. R., 2001, "Nonlinear Transient Behavior of a Sliding System with Frictionally Excited Thermoelastic Instability," *ASME J. Tribol.*, **123**, pp. 699–708.
- [9] Kennedy, F. E., and Ling, F. F., 1974, "A Thermal, Thermoelastic and Wear Simulation of a High Energy Sliding Contact Problem," *ASME J. Lubr. Technol.*, **96**, pp. 497–507.
- [10] Afferrante, L., Ciavarella, M., Decuzzi, P., and Demelio, G., 2003, "Transient Analysis of Frictionally Excited Thermoelastic Instability in Multi-Disk Clutches and Brakes," *Wear*, **254**, pp. 136–146.
- [11] Martins, J. A. C., Guimaraes, J., and Faria, L. O., 1995, "Dynamic Surface Solutions in Linear Elasticity and Viscoelasticity With Frictional Boundary Conditions," *J. Vib. Acoust.*, **117**, pp. 44–451.
- [12] Adams, G. G., 1995, "Self-excited Oscillations of Two Elastic Half-Spaces Sliding With a Constant Coefficient of Friction," *ASME J. Appl. Mech.*, **62**, pp. 867–872.
- [13] Kinkaid, N. M., O'Reilly, O. M., and Papadopoulos, P., 2003, "Automotive Disc Brake Squeal," *J. Sound Vib.*, **267**, pp. 105–166.
- [14] Moirot, F., and Nguyen, Q. S., 2000, "Brake Squeal: A Problem of Flutter Instability of the Steady Sliding Solution?" *Arch. Mech.*, **52**, pp. 645–662.
- [15] Ouyang, H., Cao, Q., Mottershead, J. E., and Treyde, T., 2003, "Vibration and Squeal of A Disc Brake: Modelling And Experimental Results," *Proceedings of The Institution of Mechanical Engineers Part D-Journal of Automobile Engineering*, **217**, pp. 867–875.
- [16] Afferrante, L., Ciavarella, M., and Barber, J. R., 2006, "Sliding Thermoelastodynamic Instability," *Proc. R. Soc. London, Ser. A*, **462**, pp. 2161–2176.
- [17] Yi, Y. B., Du, S. Q., Barber, J. R., and Fash, J. W., 1999, "Effect of Geometry on Thermoelastic Instability in Disk Brakes and Clutches," *ASME J. Tribol.*, **121**, pp. 661–666.